Journal of Applied Polymer Science

Electrochemical Synthesis of Nanostructured Polyaniline: Heat Treatment and Synergistic Effect of Simultaneous Dual Doping

Subhendu Bhandari, Nikhil Kumar Singha, Dipak Khastgir
Indian Institute of Technology, Kharagpur, West Bengal 721302, India
Correspondence to: D. Khastgir (E-mail: khasdi@rtc.iitkgp.ernet.in)

ABSTRACT: Different nanostructured polyaniline (PAni) has been synthesized via facile template-free electrochemical synthesis approach in aqueous medium. Instead of conventionally used aniline, aniline sulphate was used in electrochemical polymerization. The synthesis process involves simultaneous doping with combination of inorganic and organic acid, i.e., sulfuric acid (H_2SO_4) and *p*-toluenesulfonic acid (PTSA) at different ratios keeping total dopant concentration constant. Synergistic increase in conductivity is observed and the best conductivity is achieved at 3:1 ratio of [H_2SO_4]:[PTSA]. Different nanostructures of PAni are revealed through morphological analysis consisting of nanosphere, nanorod, and clustered particles among which finer nanorods show the best electrical conductivity. Upon controlled heat treatment followed by further cooling, resistivity increases, but after one day it decreases again and in the optimized dual doped PAni, it approaches approximately the same value of initial resistance. Lattice strain and benzenoid to quinonoid ratio increases with heat treatment. © 2012 Wiley Periodicals, Inc. J. Appl. Polym. Sci. 129: 1264–1273, 2013

KEYWORDS: conducting polymers; nanostructured polymers; spectroscopy; morphology; structure-property relations

Received 30 August 2012; accepted 3 November 2012; published online 27 November 2012
DOI: 10.1002/app.38803

INTRODUCTION

Among intrinsically conducting polymers (ICP), polyaniline (PAni) attracted much attention of researchers because of its unique electrical properties in a wide range, low cost of monomer, and good environmental stability. Compared to chemically synthesized polymers, electrochemically synthesized polymers give more purity due to use of only monomer and electrolyte. Doping of conducting polymers increases its conductivity. Doping is carried out by means of either (1) redox doping where oxidizing or reducing agent add or remove electron to or from polymer backbone or (2) protonic acid doping where number of electron in the polymer backbone remains unchanged. Often, more than one dopant is used to have synergistic effect on conductivity of the polymer. Use of two dopants separately is called dual doping or secondary doping especially where the solvent acts as secondary dopant and apparently "inert" e.g. *m*-cresol. Secondary doping may change the arrangement and conformations of the macromolecular chain of polyaniline.[1] Choice of good solvent as secondary dopant is important which increase conductivity through increases in local structural order.[2–5] Cao et al. reported that polyaniline doped with CSA and cast from *m*-cresol shows 10^3 times higher conductivity than that cast from chloroform where *m*-cresol acts as secondary dopant.[3–6] Secondary doping of PAni is reported in several cases with different primary/secondary dopant combinations e.g. camphor sulfonic acid (CSA)/*m*-cresol,[7] dodecyl benzene sulfonic acid (DBSA)/*m*-cresol,[8] sulfophthalic acid/sodium laurylsulphate,[9] fluoroboric acid (HBF_4)/dodecylhydrogen sulfate (DHS),[10] and so forth. Effect of different reaction parameters for electrochemical synthesis of PAni was also reported.[11] According to available literatures, nanostructured PAni has not yet been synthesized from aniline sulphate and also simultaneous dual doping of PAni by means of electropolymerization has not been done earlier. In this study, nanostructured PAni with different morphologies were synthesized using a template free novel electrochemical method using both organic acid (PTSA) and inorganic acid (H_2SO_4) dopants simultaneously at the time of synthesis instead of commonly used process of post-synthesis dedoping followed by redoping. In earlier studies, changes in structural change and electrical properties during heat treatment of polyaniline were investigated,[12–14] but the effect of heat treatment followed by cooling of dual doped PAni is not reported so far. Here, for the first time we have studied the heating and cooling effect on dual doped system which is influenced by size and type of dopant differently. PAni is synthesized either using template[15] or through template free[16–18] process. Depending on different dopants and reaction conditions, morphology of PAni varies widely[19] from rice-grain,[20] plate,[21] spherical[22] or microporous,[23] to microspheres.[24] template synthesized nanotubes, nanofibers and nanowires,[25–27] or template-free nanofibers[28] and self-assembled nanotubes.[29] Formation of PAni

Table I. Sample Designation, Composition, and Properties Calculated From Different Characterization Techniques

	Composition		Properties			
			XRD			TEM (SAD)
Sample[a] code	Conc^{n} of H_2SO_4 (M)	Conc^{n} of PTSA (M)	Angle (2θ)	Relative intensity (%)	*d*-spacing (Å)	*d*-spacing (Å)
P_0	0	0	25.3	100	3.52	2.68
P_{40}	1	0	25.2	100	3.53	3.40
P_{31}	0.75	0.25	25.7	72.5	3.45	2.84
P_{22}	0.5	0.5				
P_{13}	0.25	0.75				
P_{04}	0	1	25.2	98	3.52	3.31

[a]Subscript in the form of *xy* denotes the addition of x parts of H_2SO_4 and y parts of PTSA.

nanofibers and nanotubes with different doping agents in water have been studied.[30]

Wan and coworkers[31] prepared H_3PO_4, H_2SO_4, HCl, and HBF_4 doped PAni and have shown that PAni has granular morphology when [acid]/[aniline] $\leq$ 2 and fibrous nanostructures at [acid]/[aniline] $\leq$ 0.5 whereas, in this study, different morphologies were obtained at [acid dopant]/[aniline sulphate] = 1 with varying proportion of the dopants. General formula of PAni is $[(-B-NH-B-NH-)_y(-B-N=Q=N-)_{1-y}]_x$ where B represents a benzenoid ring while Q represents a quinonoid ring. Conducting emeraldine state of PAni is typically 50% oxidized. Here, we have studied the change in benzenoid to quinonoid ratio in case of single and dual doped PAni and also its change with heat treatment.

In this study, PAni was electrochemically synthesized from aniline sulphate and dual doped with H_2SO_4 and PTSA at the time of synthesis individually and together in different proportions keeping the total acid concentration same. Till date, we could not find published report on synthesis of nanostructured PAni from aniline sulphate. Aniline sulphate is a white colored powder which is highly soluble in water and less hazardous than aniline. Since, *in-situ* dual doping was carried out instead of redoping of PAni after dedoping, partial doping occurs in this case. Controlled heating followed by cooling was carried out to study the effect of heat treatment of dual doping. Electrical properties were measured for all the samples by means of AC conductivity temperature dependent DC conductivity was also measured. The samples were characterized by Fourier transform infrared spectroscopic (FTIR) analysis. X-ray diffraction (XRD) analysis of the powder samples shows the changes in crystallinity. Different nanostructures of PAni like rod, sphere, ribbon, etc. were obtained in scanning electron microscopy (SEM) and transmission electron microscopy (TEM) analysis.

EXPERIMENTAL

Materials

Aniline (analytical grade) and sulfuric acid were obtained from Merck, India; *p*-toluenesulfonic acid was purchased from Spectrochem, India. All the materials were used as received. Graphite plate of dimension 14.5 cm × 5 cm × 0.5 cm was used as working electrode, copper plate of dimension 15 cm × 5 cm × 0.05 cm was used as counter electrode, and a saturated calomel electrode (SCE) was used as reference electrode.

Electrochemical Synthesis of In-situ Dual Doped PAni

Aniline was taken in water and stirred vigorously. It was then reacted to sulfuric acid. White precipitate of aniline sulphate

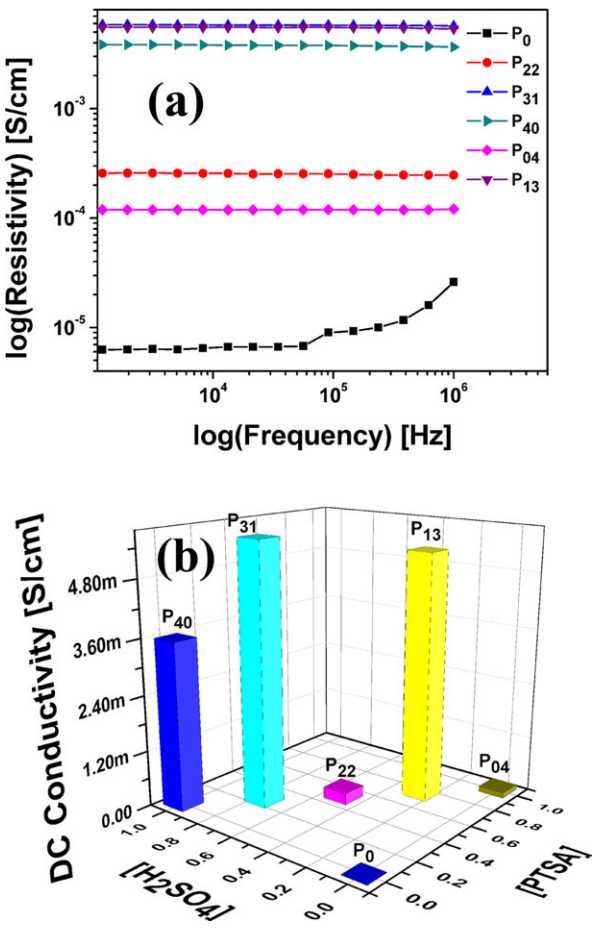

Figure 1. (a) AC conductivity and (b) DC conductivity of simultaneous dual doping of polyaniline electrochemically synthesized with varying dopant ratio $[H_2SO_4]$:[PTSA] = 0:0 (P_0), 4:0 (P_{40}), 3:1 (P_{31}), 2:2 (P_{22}), (c) 1:3 (P_{13}), and (d) 0:4 (P_{04}). [Color figure can be viewed in the online issue, which is available at wileyonlinelibrary.com.]

Applied Polymer SCIENCE

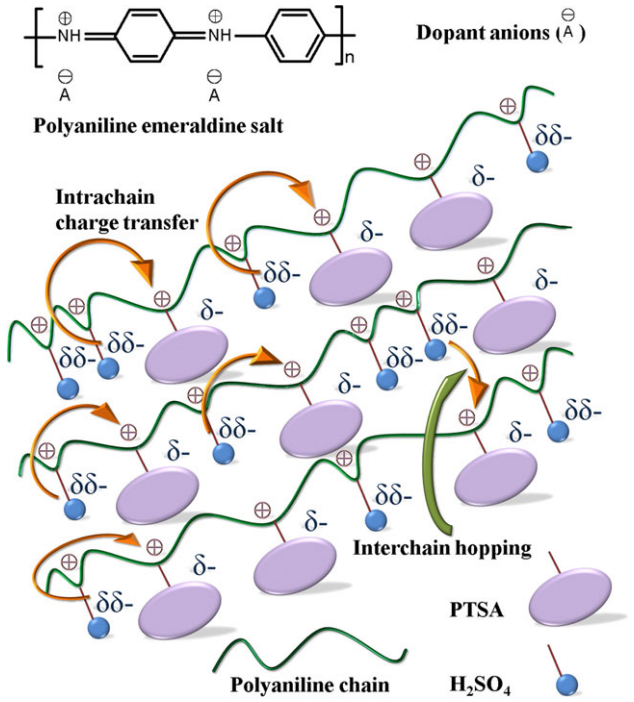

Scheme 1. Schematic presentation of proposed working method of simultaneous dual doping of PAni. [Color figure can be viewed in the online issue, which is available at wileyonlinelibrary.com.]

was filtered and dried in oven. Electrochemical polymerization of PAni was carried out from 0.5*M* aniline sulphate in water medium (100 mL) taken in a single-compartment cell with *in-situ* doping with H_2SO_4 and PTSA keeping the total dopant concentration constant at 1*M* and the ratio of the concentration of [H_2SO_4]:[PTSA] was varied at 1:3, 1:1, and 3:1. During synthesis, copper plate was used as cathode and graphite plate as anode. Constant current of 0.05 Å versus SCE was applied for

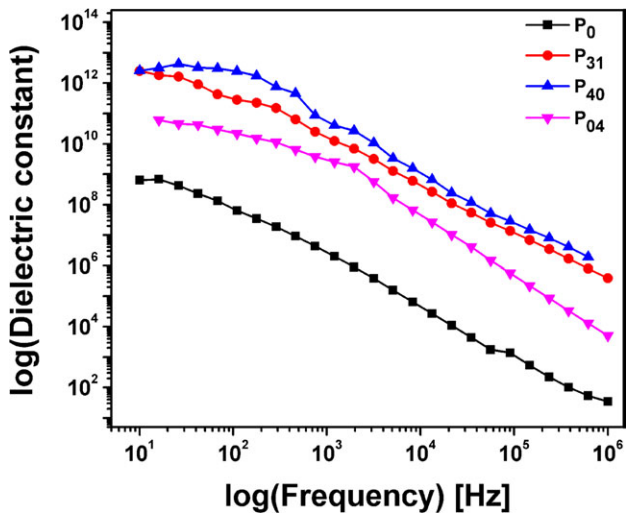

Figure 2. Dielectric constant of simultaneous dual doping of polyaniline electrochemically synthesized with varying dopant ratio [H_2SO_4]:[PTSA] = 0:0 (P_0), 4:0 (P_{40}), 3:1 (P_{31}), and (d) 0:4 (P_{04}). [Color figure can be viewed in the online issue, which is available at wileyonlinelibrary.com.]

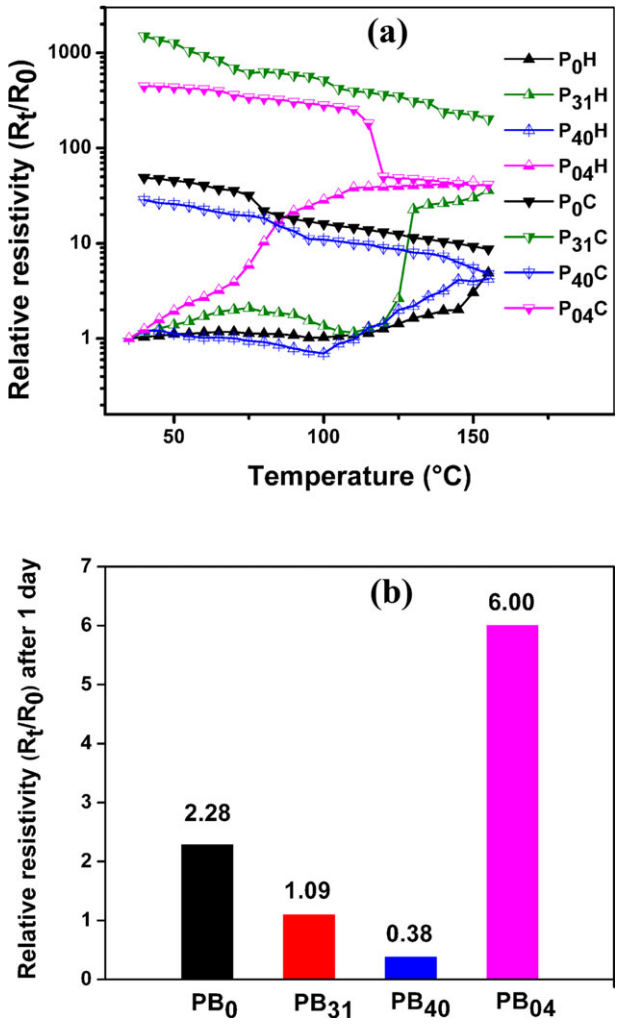

Figure 3. (a) Temperature dependent relative resistivity of polyaniline in heating and cooling cycle (H stads for heating and C stands for cooling cycle), (b) relative resistivity after 1 day of heat treatment. [Color figure can be viewed in the online issue, which is available at wileyonlinelibrary.com.]

an hour, thereafter the polarity of the electrodes were changed and the process continued for 30 min and this process was further repeated twice to get the final product. All the reactions for synthesis of both aniline sulphate and PAni were carried out at room temperature. After preparation, formed PAni was filtered and washed with deionized water, methanol, and ethanol to remove the oligomers followed by drying at 50°C.

Characterization

Electrical Properties. AC resistance was measured with Quadtech 7600 Precision LCR Meter (Model-B). DC resistance was measured with Agilent 34401A 6½ Digit Multimeter. For both AC and DC resistance measurements, two circular copper plate electrodes of area 3.8476 cm^2 were used. Both AC and DC conductivity were calculated using the equation $\sigma = t/(A.R)$ where σ is conductivity (S), t is the thickness of the sample (cm), A is the are of the electrode (3.8476 cm^2), and R is the measured resistance (Ω). Temperature-dependant relative resistivity was measured with Agilent 34401A 6½ Digit Multimeter and a

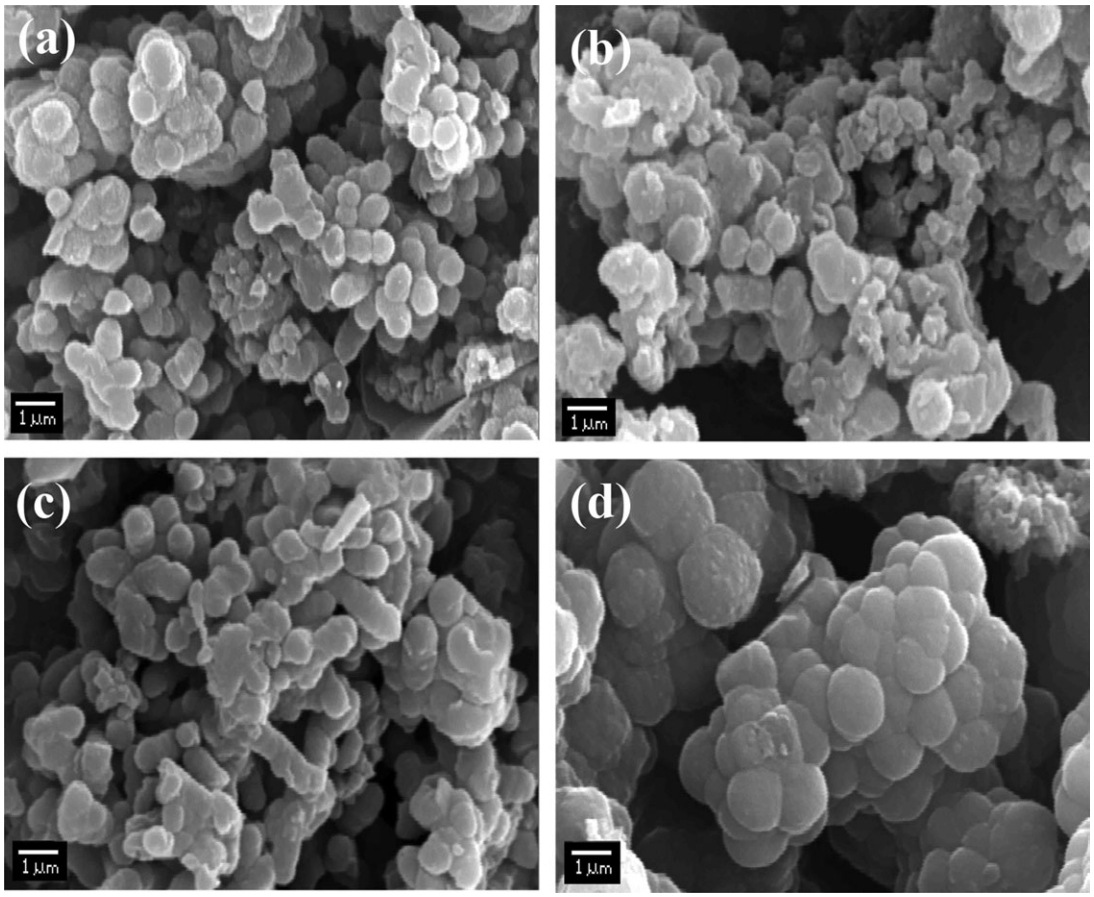

Figure 4. SEM micrograph of polyaniline electrochemically synthesized with varying dopant ratio $[H_2SO_4]$:[PTSA] = (a) 0:0 (P_0), (b) 3:1 (P_{31}), (c) 4:0 (P_{40}), and (d) 0:4 (P_{04}).

heating element (S.C. Dey & Co.) using the equation $R_i = R_t/R_0$; where R_i is relative resistance, R_t is resistance at temperature t°C, and R_0 is initial resistance at room temperature.

FTIR Analysis. The FTIR spectra of the PAni samples were recorded using a Perkin-Elmer (model-837) FTIR spectrometer, Spectrum RX 1, USA, from the KBr pellet of PAni. KBr pellet was prepared from the mixture of PAni and KBr under 10 N load.

X-ray Diffraction Analysis. X-ray diffraction (XRD) was carried out with Cu detector using an X-ray wavelength of 1.54 Å. For analysis, X'Pert PRO, PANalytical instrument, USA software was used. Estimation of *d*-spacing was done using the Bragg equation:

$$n\lambda = 2d \sin\theta$$

where n is an integer, λ is the wavelength of the incident X-ray which is 54 Å for Cu target, d is the d-spacing, and θ is the angle between incident beam and scattering planes.

Crystallite size was evaluated using the Scherrer formula:[32]

$$D = \frac{K\lambda}{B\cos\theta}$$

where D is the crystallite size, K is the shape factor for the average crystallite (~0.9), B is the full width at half maximum in radian.

Lattice strain was calculated using Williamson-Hall equation:[32,33]

$$B\cos\theta = \frac{K\lambda}{D} + 4\varepsilon\sin\theta$$

where ε is lattice strain.

Morphology Analysis. Morphology of the synthesized PAni samples was analyzed using scanning electron microscopy (SEM) and high-resolution transmission electron microscopy (HRTEM). SEM was done in JEOL JSM 5800, JEOL, Japan. Gold coating was done onto PAni powder samples prior to SEM analysis. HRTEM was carried out in JEOL JEM 2100 instrument. For TEM analysis, PAni powder samples were taken in tetrahydrofuran (THF) and sonicated in IMECO (1060-02) ultrasonicator for 1 h prior to put it on copper grid and. Apart from morphological pictures, selected area diffraction (SAD) diagrams were also taken to study the crystallinity in PAni samples. From SAD diagrams, d-spacing was calculated and compared with that obtained from XRD.

Thermogravimetric Analysis. Thermogravimetric analysis (TGA) was carried out using TGA, Q 50 from TA Instruments, USA in N_2 atmosphere from room temperature to 600°C at 20°C/min heating rate.

Applied Polymer SCIENCE

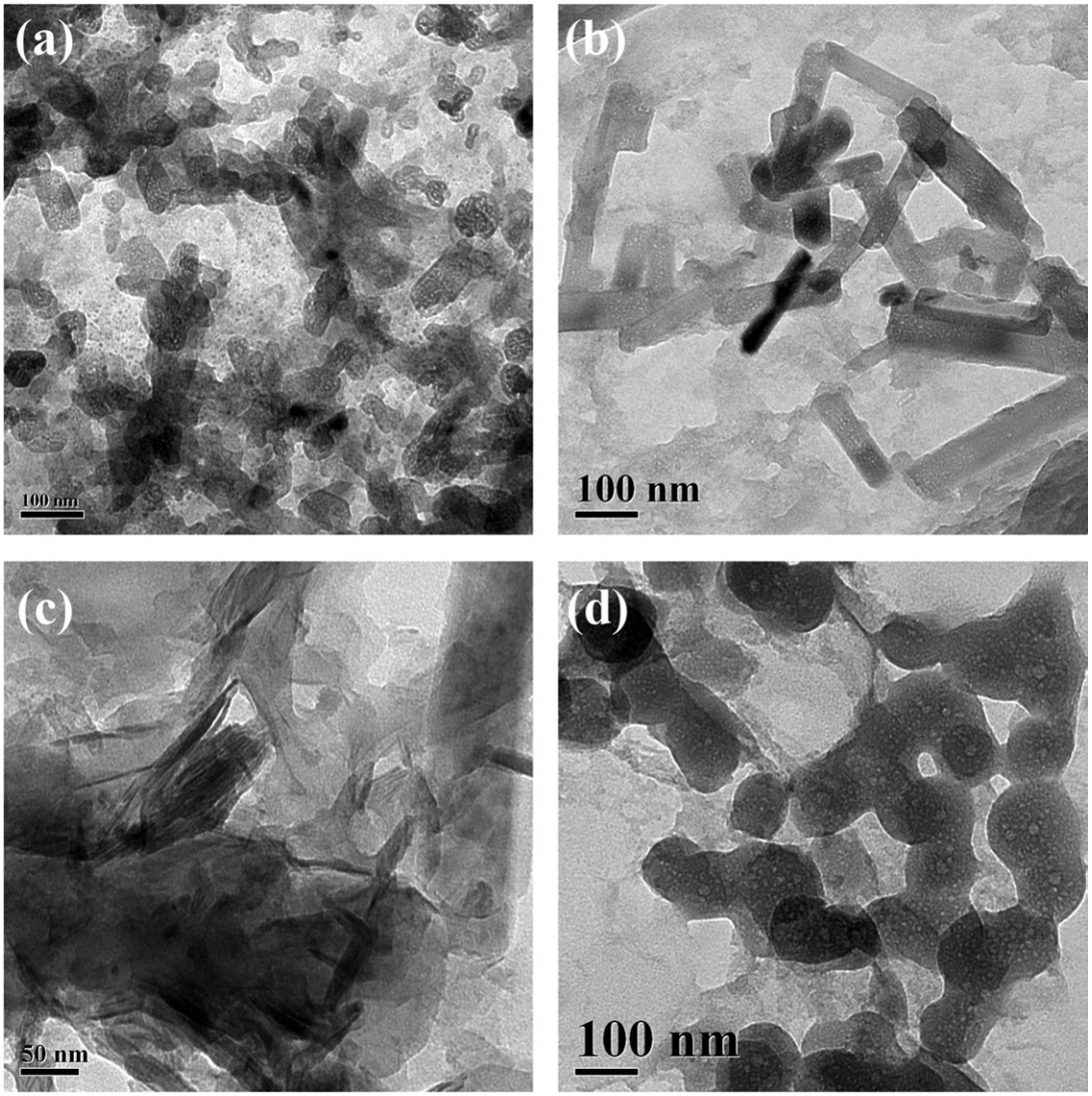

Figure 5. TEM micrograph of polyaniline electrochemically synthesized with varying dopant ratio $[H_2SO_4]$:[PTSA] = (a) 0:0 (P_0), (b) 3:1 (P_{31}), (c) 4:0 (P_{40}), and (d) 0:4 (P_{04}).

RESULTS AND DISCUSSION

Sample designations and compositions are presented in Table I. It also contains structural characteristics of different PAni samples obtained from XRD, TEM, and FTIR analysis.

Electrical Properties

It is found that AC conductivity [Figure 1(a)] is mostly frequency independent which reveals that, main contribution of AC conductivity is from DC conductivity [Figure 1(b)] in accordance with the formula $\sigma_{AC} = \sigma_{DC} + 2\pi\varepsilon''$ where σ_{AC} is the AC conductivity, σ_{DC} is the DC conductivity, f is the frequency of measurement, and ε'' is the loss factor.[12] The highest conductivity is observed for sample P_{31} (doped with 25% H_2SO_4 and 75% PTSA) followed by $P_{13} > P_{40} > P_{22} > P_{04}$. Type of dopant used has a significant effect on conductivity compared to doped with PTSA. However, when dual doping is done using suitable proportion of H_2SO_4:PTSA as in the case of P_{31} and P_{13} higher conductivity than both P_{40} (H_2SO_4 doped) and P_{04} (PTSA doped) is observed that confirms the synergistic effect of dual doping on electrical conductivity. On contrast, the conductivity of P_{22} is intermediate between P_{40} and P_{04} which indicates that equal proportion of the dopants does not lead to synergistic increase in conductivity, rather in such case, the competing effect of the dopants is observed. However, PAni sample without external dopant (P_0) shows the least conductivity and some frequency dependency especially at high frequency region beyond 10^4 Hz.

When PAni is doped with two dopants simultaneously, both of the counter ions get attached to polymer chain, but when their positions on the running chain occur alternately there will be alternate distribution of the charge density. Unequal distribution of counterions may vary the difference in charge density. This, in turn may facilitate intramolecular charge transport and intermolecular hopping giving rise in synergistic increase in conductivity as seen in P_{31} and P_{13} (Scheme 1). But, if an equal proportion of dopant is used as in P_{22}, the distribution of

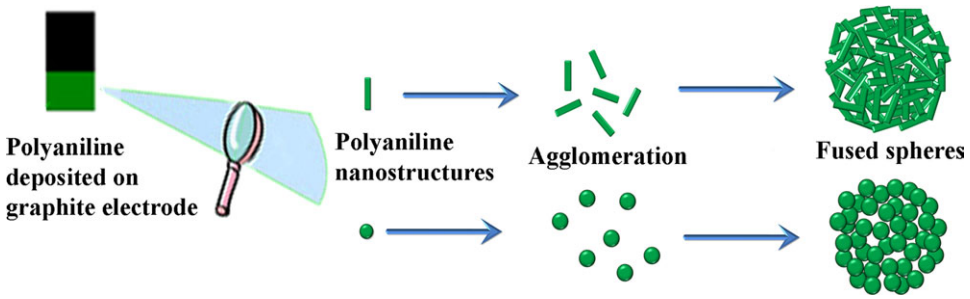

Scheme 2. Schematic diagram of formation of agglomerates from nano particles to form macro structure of polyaniline electrochemically synthesized with varying dopant ratio [H_2SO_4]:[PTSA] = 4:0 (P_{40}), 3:1 (P_{31}), 0:4 (P_{04}), and 0:0 (P_0). [Color figure can be viewed in the online issue, which is available at wileyonlinelibrary.com.]

counterions becomes more uniform resulting in less difference in charge density. Thus, instead of synergistic effect the competing effect of the dopants prevails to give intermediate conductivity. Considering the level of conductivity, PAni samples P_{20}, P_{31}, P_{40}, and P_{04} were selected for further investigation. The dual doped sample P_{31} was selected in contrast to P_{22} and P_{13} because it shows higher conductivity than the other two. log–log plots of permittivity versus frequency show that for all PAni samples permittivity decreases with increase in frequency almost linearly. With the change in polarity of applied AC field, dipoles

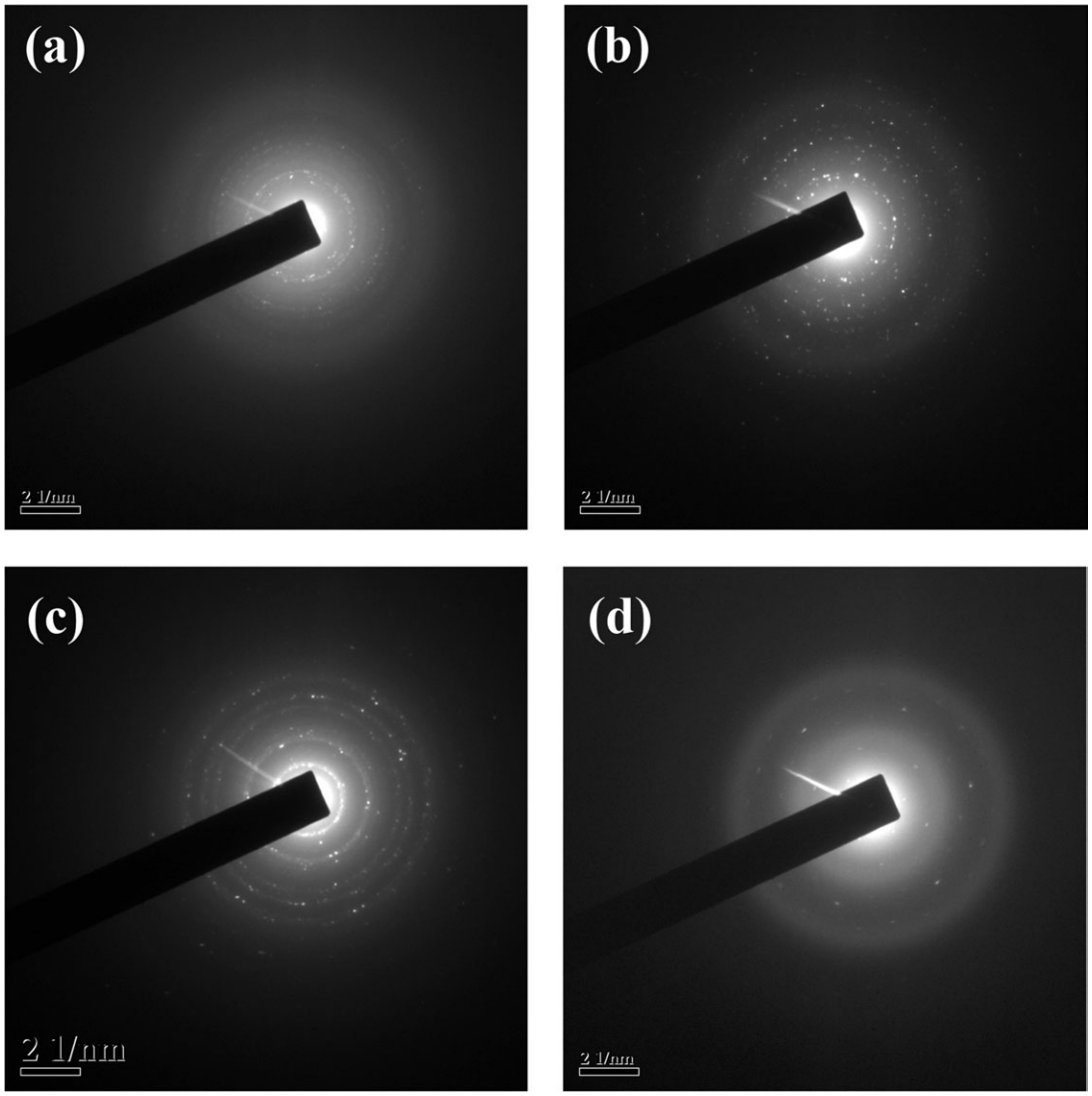

Figure 6. SAD (HRTEM) images of polyaniline electrochemically synthesized with varying dopant ratio [H_2SO_4]:[PTSA] = (a) 0:0 (P_0), (b) 3:1 (P_{31}), (c) 4:0 (P_{40}), and (d) 0:4 (P_{04}).

Applied Polymer SCIENCE

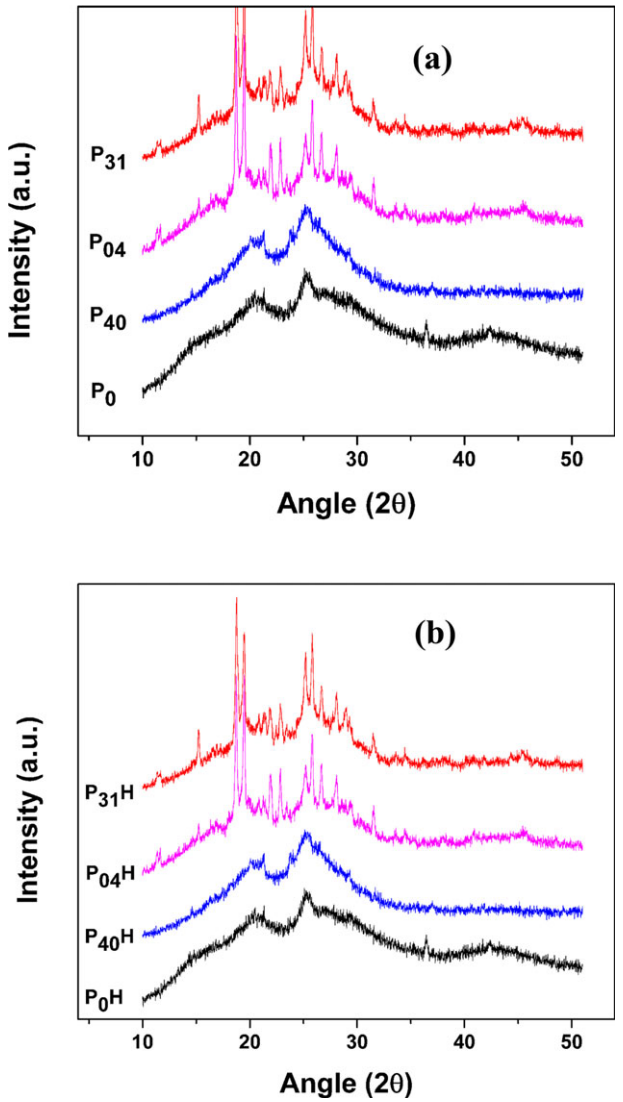

Figure 7. XRD pattern of polyaniline (a) electrochemically synthesized with varying dopant ratio $[H_2SO_4]$:[PTSA] = 4:0 (P_{40}), 3:1 (P_{31}), 0:4 (P_{04}), and 0:0 (P_0) before heat treatment and (b) after heat treatment. [Color figure can be viewed in the online issue, which is available at wileyonlinelibrary.com.]

reorient themselves. At higher frequency, dipoles fail to follow the polarity change of electric field consequently; dielectric constant decreases (Figure 2).

Temperature dependent relative resistivity plot [Figure 3(a)] shows that except PTSA doped PB_{04}, in case of other three samples, change in relative resistivity is less up to 100°C and then it increases fast whereas in PB_{04}, it increases from 70°C. This change may be due to oxidation during heating and also due to loss of dopants and moisture, part of which may act as dopant. Loss of dopants with increase in temperature is temporary and after cooling relative resistivity increases, because within short time of cooling, dopants cannot recombine with the polymer chain and internal disorder increases which in turn increase the relative resistivity. But after 1 day relative resistivity R_i comes down drastically to <10 from the range of 30–1500 [Figure 3(b)]. After sufficient time is given, temporarily detached dopants are allowed for relaxation to find suitable place to recombine with the polymer chain which again decreases resistivity. Dopants of small size (H_2SO_4) rearrange their position more suitably and in some cases like PB_{40}, it decreases resistivity even lower than initial value at room temperature. But, larger dopants (PTSA) cannot rearrange easily. Thus in PB_{04} relative resistivity is comparatively higher (~6) than PB_{31}.

Morphology

It is evident from SEM micrographs (Figure 4) that, in all preparation methods, the end products are clustered particles of PAni having more or less spherical structure (0.3–0.7 μm). However, HRTEM pictures (Figure 5) reveal the presence of different nanoparticles in the clustered particles. P_0 particles show oval shaped morphology (<60 nm). P_{40} particles have layered flake like and P_{04} particles have sphere and dumble like (~100 nm) while P_{31} particles show rod like morphology (length ~ 150–300 nm and dia. ~ 30–70 nm) [Figure 5(b)]. Thus, it is confirmed that using suitable proportion of dopant without changing total dopant concentration generates new type of nanostructure which is completely different from individually doped PAni. These nanoparticles agglomerate[34] (Scheme 2) to form larger granules (0.5–1.5 μm), as seen in the SEM pictures. It is interesting to note that the morphology depends on the relative proportion of two dopants used. Although the reason behind this difference is not clearly understood, it is assumed that during simultaneous doping both the dopants try to get attached at suitable position in the PAni chain. Consequently, the dopants are arranged in alternating fashion during PAni synthesis which gives rise to linear (unidirectional) formation of PAni, as a result, rod-like nanostructure of PAni is obtained. Moreover, plasticizing effect of PTSA and the difference in nucleation process occurring for different dopant ratios may play some role in the formation of different types of nanostructured particles. According to earlier investigations,[35,36] formation of PAni nucleation sites on electrode surface is independent of applied potential. In this study, since total anion concentration and reaction time are the same in all the cases, 2D growth in P_{40} forming flake/layer structure and 1D growth

Table II. Structural Characteristics of PAni Before and After Heat Treatment

Sample code	Temperature[a] (°C)	B:Q	Crystallite size (Å)	Lattice strain (%)
P_0	30	55:45	58	2.716
P_{31}	30	43:57	284	0.547
P_{40}	30	47:53	163	0.975
P_{04}	30	40:60	125	1.280
P_0H	150	38:62	44	3.618
$P_{31}H$	150	49:51	243	0.653
$P_{40}H$	150	48:52	147	1.071
$P_{04}H$	150	48:52	244	0.651
$PB_{31}HH$	450	62:38		

[a]Temperature of heat treatment.

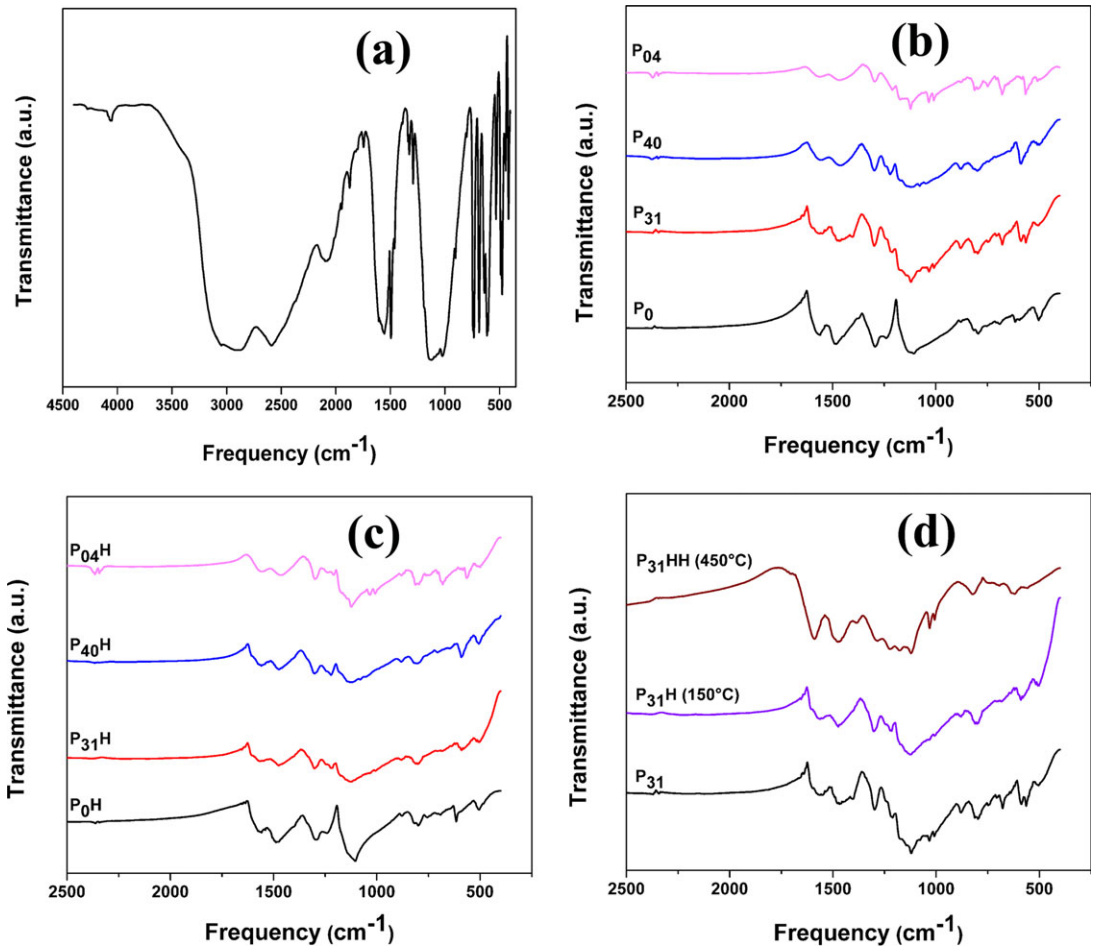

Figure 8. FTIR spectra of (a) aniline sulphate, (b) PAni electrochemically synthesized with varying dopant ratio [H_2SO_4]:[PTSA] = 4:0 (P_{40}), 3:1 (P_{31}), 0:4 (P_{04}), and 0:0 (P_0) before heat treatment, (c) after heat treatment at 150°C, and (d) after heat treatment of optimized doped P_{31} at different temperatures. [Color figure can be viewed in the online issue, which is available at wileyonlinelibrary.com.]

in P_{31} forming nanorod structure may not be attributed to progressive and instantaneous nucleation followed by 2D and 1D growth respectively as reported in literatures.[36,37] Rather, in this case, the difference in morphology arises may be due to the effect of the two dopants as explained earlier and the resulting complexity in nucleation process which is not understood clearly. The selected area diffraction (SAD) pictures (Figure 6) show number of concentric rings consisting of white spots which indicates partial crystallinity. Less number of spots for P_{04} indicates that it is more amorphous compared to P_{40} where latter has distinct rings due to presence of more number of crystal layers. Large number of distinct spots in dual doped sample P_{31} is due to formation of more crystallites. From the SAD patterns, d-spacings for different PAni samples were calculated and compared with those obtained from XRD, as shown in Table I; values obtained from two experiments are close enough.

X-ray Diffraction

In XRD patterns of different samples two broad peaks are observed at 2θ ~ 20° and 25° (Figure 7). The peak centered at 2θ ~ 20° is ascribed to periodicity parallel to the polymer chain, while the latter is due to the periodicity perpendicular to the polymer chain.[38] The doping increases crystallite size. Doping with H_2SO_4 (P_{40}) shows larger crystallite size than that with PTSA (P_{04}). Although dual doped sample (P_{31}) shows the largest crystallite size, for PTSA, the higher bulkiness of counter ion compared to that of H_2SO_4 increases the lateral distances among neighboring chains which in turn reduces the compactness of PAni chains leading to decrease in crystallinity for PAni-PTSA compared to PAni-H_2SO_4. Peak broadening arising due to higher lattice strain and smaller crystallite size is the highest in P_0 and the lowest in P_{31} (H_2SO_4/PTSA doping ration 3:1) whereas, P_{40} (H_2SO_4 doped) and P_{04} (PTSA doped) exhibits intermediate result between these two.[39] Heat treatment breaks the larger crystal structures into smaller one [Figure 7(b)] which results in decrease in crystallite size and increase in lattice disorder; consequently lattice strain increases (Table II). A reverse trend is observed in case of PTSA doped PB_{04} where after heat treatment, crystallite size increases. Lattice strain is the lowest in PB_{31} which indicates formation of more stable crystallites with less lattice disorder and more conducting networks which increases conductivity.[39]

Applied Polymer SCIENCE

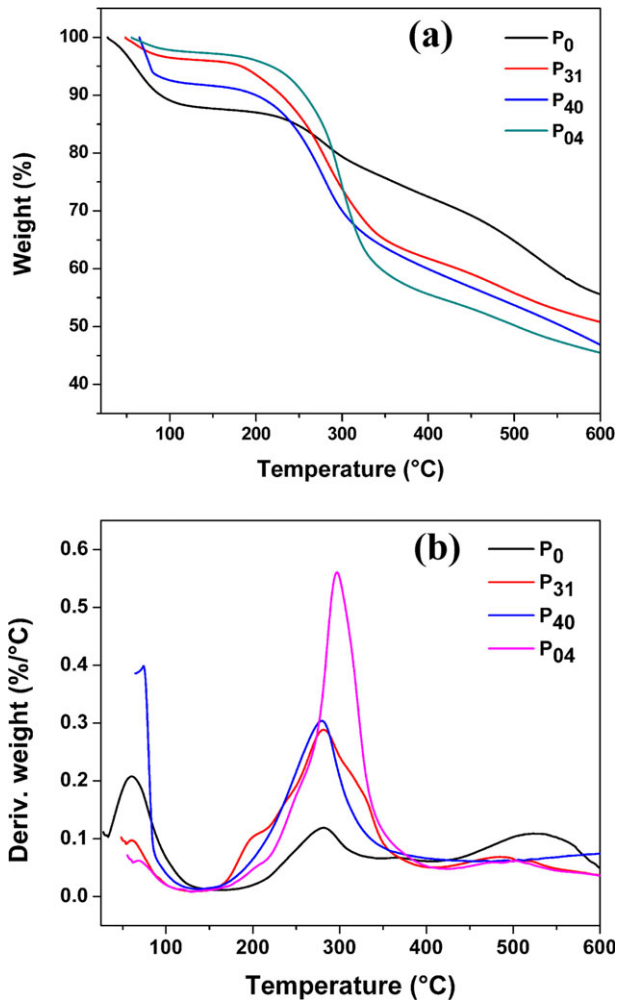

Figure 9. (a) TGA and (b) DTG curves of polyaniline electrochemically synthesized with varying dopant ratio [H_2SO_4]:[PTSA] = 4:0 (P_{40}), 3:1 (P_{31}), 0:4 (P_{04}), and 0:0 (P_0). [Color figure can be viewed in the online issue, which is available at wileyonlinelibrary.com.]

FTIR Spectroscopy

Figure 8(a) shows the FTIR spectra of aniline sulphate. The bands at 1494 and 1462 cm^{-1} are assigned to the phenyl ring. NH_2 scissoring and waging vibrations appear at 1608 and 606 cm^{-1}. Peaks at 1337, 1327, and 1291 cm^{-1} are due to the presence of phenyl-nitrogen bond. Deformation bands for S=O_2 group appear at 532 and 444 cm^{-1}.[40] As shown in FTIR spectra for different samples [Figure 8(b)] the absorption band at 1295 cm^{-1} corresponds to π electron delocalization induced in the polymer through protonation or C—N—C stretching vibration. The band at 1243 cm^{-1} is the characteristic of C—N stretching vibration in the polaron structure. The 1138 cm^{-1} band is assigned to the vibration mode of the —NH in the protonated emeraldine base (B-NH^+=Q).[11] The band at 808 cm^{-1} is for C—H out of plane deformation of 1,4-disubstituted benzene rings. The characteristic peaks at 1466 cm^{-1} and 1631 cm^{-1} are attributed respectively to benzenoid (B) and quinonoid (Q) ring stretching. B:Q ratio is the highest in case of P_0 (Table II) which decreases with doping. Dual doped P_{31} has an intermediate value of B:Q compared to H_2SO_4 doped P_{40} and PTSA doped P_{04}. After heat treatment, B:Q ratio decreases in case of P_0 [Figure 8(c)] whereas, it increases for the doped samples. This may be due to structural interchanging of benzenoid and quinonoid structures on application of heat. Benzenoid structure converts to quinonoid more in the case of P_0 whereas, dopants attached with benzenoid structures resists to change in quinonoid structure in case of doped samples due to which in these cases, B:Q ratio increases. This interchange also changes the conductivity to a great extent. After heat treatment at 150°C, B:Q ratio is almost the same for different doped samples [Figure 8(d)] which infers that upon heat treatment of different PAni doped at constant dopant concentration, B:Q ratio increases to the same level irrespective of type of dopants. Structural interchange happens while heat is applied to the polymer. To study the structural interchange in a particular sample, P_{31} was heated at 450°C (P_{31}HH). It is found that following the trend as obtained earlier; here also at 450°C benzenoid to quinonoid conversion is more than that at 150°C (Table II) which proves that the conversion from benzenoid to quinonoid continues even at higher temperature.

Thermogravimetric Analysis

To gain insight into the thermal degradation characteristics, thermogravimetric analysis for PAni samples were done. In all cases, three-stage degradation is observed [Figure 9(a)]. The first stage of degradation is due to loss of moisture. Loss of moisture is the highest in P_{04} and lowest in P_0 whereas, extent of moisture loss for dual doped P_{31} is intermediate between P_{40} and P_{04}. The second stage of degradation (170–370°C) is due to loss of dopants.[12] From DTG graph [Figure 9(b)], it is clear that the rate of dopant loss with increase in temperature is the highest in PTSA doped P_{04} because of weaker interaction of organic acid dopant PTSA compared to organic acid dopant H_2SO_4 whereas, that of dual doped P_{31} is even less than both these two individually doped PAni. In case of P_{31}, degradation at 600°C is better (49.5%) than both P_{40} (53.8%) and P_{04} (54.8%).

CONCLUSIONS

A facile template free electropolymerization approach to synthesize different nanostructured PAni in aqueous medium is described here which involves aniline sulphate instead of conventionally used aniline. Electrochemical synthesis was successfully carried out in aqueous medium. Formation of PAni is confirmed from spectroscopic studies. Simultaneous dual doping with mixed organic/inorganic acid system carried out during electropolymerization exhibits synergistic improvement in conductivity in certain cases. Resistivity increases during both heat treatment and further cooling, but after given sufficient time for relaxation of the dopants, resistivity decreases to a great extent. With varying dopant ratio at constant total dopant concentration, different nanostructures were obtained which agglomerates to form larger microspheres. At the optimum proportion of dopant, nanorod-like morphology and the formation of more crystallites are observed which also exhibits the lowest lattice strain and the slowest rate of temperature dependent dopant loss. Benzenoid to quinonoid ratio increases with heat treatment but the ratio is almost independent of ratio of dopants.

REFERENCES

1. MacDiarmid, A. G.; Epstein, A. *J. Synth Met* **1995**, *69*, 85.
2. Epstein, A. *J. Springer Ser Mater Sci* **2001**, *41*, 3.
3. MacDiarmid, A. G.; Epstein, A. *J. Synth Met* **1994**, *65*, 103.
4. Xia, Y.; Wiesinger, J. M.; MacDiarmid, A. G.; Epstein, A. *J. Chem Mater* **1995**, *7*, 443.
5. Min, Y.; Xia, Y.; MacDiarmid, A. G.; Epstein, A. *J. Synth Met* **1995**, *69*, 159.
6. Cao, Y.; Smith, P.; Heeger, A. *J. Synth Met* **1992**, *48*, 91.
7. Tigelaar, D. M.; Lee, W.; Bates, K. A.; Saprigin, A.; Prigodin, V. N.; Cao, X.; Nafie, L.; Platz, M. S.; Epstein, A. *J. Chem Mater* **2002**, *14*, 1430.
8. Wei, L.; Chen, Q.; Gu, Y. *Synth Met* **2010**, *160*, 405.
9. Sydulu, S. B.; Palaniappan, S.; Srinivas, P. *J Electrochem Soc* **2012**, *159*, A6.
10. Palaniappan, S.; Devi, S. L. *J Appl Polym Sci* **2008**, 107, 1887.
11. Bhadra, S.; Singha, N. K.; Chattopadhyay, S.; Khastgir, D. *J Polym Sci Part B: Polym Phys* **2007**, *45*, 2046.
12. Bhadra, S.; Singha, N. K.; Khastgir, D. *Polym Int* **2007**, *56*, 919.
13. Jousseaume, V.; Morsli, M.; Bonnet, A. *J Appl Polym Sci* **2002**, 84, 1848.
14. Zhang, J.; Liu, C.; Shi, G. *J Appl Polym Sci* **2005**, *96*, 732.
15. Anilkumar, P.; Jayakannan, M. *Macromolecules* **2008**, *41*, 7706.
16. Li, G.; Zhang, C.; Peng, H.; Chen, K.; Zhang, Z. *Macromol Rapid Commun* **2008**, 29, 1954.
17. Zhu, Y.; He, H.; Wan, M.; Jiang, L. *Macromol Rapid Commun* **2008**, *29*, 1705.
18. Liu, C.; Hayashi, K.; Toko, K. *Macromolecules* **2011**, *44*, 2212.
19. Marjanovic, G. C.; Konyushenko, E. N.; Trchov, M.; Stejskal, J. *Synth Met* **2008**, *158*, 200.
20. Armes, S. P.; Aldissi, M.; Agnew, S.; Gottesfeld, S. *Langmuir* **1990**, *6*, 1745.
21. Zhou, C.; Han, J.; Guo, R. *Macromolecules* **2008**, *41*, 6473.
22. Vincent, B.; Waterson, J. *J Chem Soc Chem Commun* **1990**, *9*, 683.
23. Wang, D.; Caruso, F. *Adv Mater* **2001**, *13*, 350.
24. Marie, E.; Rothe, R.; Antonietti, M.; Landfester, K. *Macromolecules* **2003**, *36*,3967.
25. Martin, C. R. *Science* **1994**, 266, 1961.
26. Martin, C. R. *Chem Mater* **1996**, *8*, 1739.
27. Wu, C. G.; Bein, T. *Science* **1994**, *264*, 1757.
28. Huang, J.; Virji, S.; Weiller, B. H.; Kaner, R. B. *J Am Chem Soc* **2003**, *125*, 314.
29. Qiu, H.; Wan, M.; Matthews, B.; Dai, L. *Macromolecules* **2001**, *34*, 675.
30. Konyushenko, E. N.; Stejskal, J.; Sedenkova, I.; Trchova, M.; Sapurina, I.; Cieslar, M.; Prokes, J. *Polym Int* **2006**, *55*, 31.
31. Zhang, Z.; Wei, Z.; Wan, M. *Macromolecules* **2002**, *35*, 5937.
32. Mote, V. D.; Purushotham, Y.; Dole, B. N. *J Theor Appl Phys* **2012**, *6*, 6.
33. Williamson, G. K.; Hall, W. H. *Acta Metallurgica* **1953**, *1*, 22.
34. Park, M. C.; Sun, Q.; Deng, Y. *Macromol Rapid Commun* **2007**, *28*, 1237.
35. John, R.; Wallace, G. G. *J Electroanal Chem* **1991**, *306*, 157.
36. K. Bade, K.; Tsakova, V.; Schultze, J. W. *Electrochim. Acta* **1992**, *37*, 2255.
37. Kemp, N. T.; Cochrane, J. W.; Newbury, R. *Synth Met* **2009**, *159*, 435.
38. Zhang, H.; Wang, J.; Wang, Z.; Zhang, F.; Wang, S. *Macromol Rapid Commun* **2009**, *30*, 1577.
39. Jeevananda, T.; Siddaramaiah, T.; Annadurai, V.; Somashekar, R. *J Appl Polym Sci* **2001**, *82*, 383.
40. Anto, P. L.; Anto, R. J.; Varghese, H. T.; Panicker, C. Y.; Philip, D.; Brolo, A. G. *J Raman Spectrosc* **2009**, 40, 1810.